Physica A 187 (1992) 456–474
North-Holland

PHYSICA A

Statistical geometry of hard particles on a sphere

S. Prestipino Giarritta
Dottorato di Ricerca in Fisica, Università degli Studi di Messina, C.P. 50, 98166 S. Agata, Messina, Italy

M. Ferrario and P.V. Giaquinta
Istituto di Fisica Teorica, Università degli Studi di Messina, C.P. 50, 98166 S. Agata, Messina, Italy

Received 14 January 1992
Revised manuscript received 14 April 1992

We present a Monte Carlo study of a two-dimensional system of hard particles embedded on the surface of a sphere. Thermodynamic and structural evidence of an ordering phase transition is found at high densities in spite of the frustration induced on the hexagonal covering by the peculiar topology of the host surface. The nature of this transition is analyzed and contrasted with the fluid–solid transition occurring in a flat geometry.

1. Introduction

The classical Landau argument about the first-order character of the melting transition is supported in three dimensions by the evidence that solids show lattice order (of low symmetry) while liquids visit mostly disordered states (the liquid phase is one of high symmetry). In two dimensions (2D) only quasi-long-range translational order may survive in the "lattice", as first shown by Peierls [1] and Landau [2] within the harmonic approximation, and by Mermin under more general hypotheses on the shape of the interaction potential [3]. If $\boldsymbol{u}(\boldsymbol{R})$ represents the deviation from equilibrium of the atom oscillating about site $\boldsymbol{R}$, then

$$\langle |\boldsymbol{u}(\boldsymbol{R}) - \boldsymbol{u}(\boldsymbol{R}')|^2 \rangle \sim \ln|\boldsymbol{R} - \boldsymbol{R}'| , \qquad \text{as } |\boldsymbol{R} - \boldsymbol{R}'| \to \infty . \tag{1.1}$$

Obviously, this fact is of little importance for finite systems [4]; however, it may be crucial if we are interested in the destiny of ideally infinite systems.

It is also worth noting that, for the very reason that in a continuous *infinite* system whose Hamiltonian is invariant under rotations and translations the density distribution functions also are Euclidean invariant (whatever the phase!), the static shear modulus does indeed vanish in the fluid as well as in the solid phase [5]. Therefore, only a localized solid may show rigidity, the property that distinguishes it from a fluid. In conclusion, since the order of the melting transition is sensitive to the extent to which the available region of phase space reduces on passing from the fluid to the solid phase, and an external field (like, for instance, the periodic boundary conditions in a simulation box) amplifies the symmetry breaking which should anyhow occur across the transition, we should expect a different behavior from finite and infinite systems, at least in two dimensions where the Landau argument loses its strength. We note here that the effect induced by boundary conditions on the shape of the transition in a finite system has been extensively discussed in relation to discrete lattice-gas models [6–8].

The above considerations suggest the possibility that certain 2D systems undergo a continuous freezing/melting transition. The widely accredited Kosterlitz and Thouless theory of the melting in two dimensions [9], later also developed by Halperin, Nelson and Young (the so called KTHNY theory) [10], confirms this feeling: in fact, the presence in the solid of dilute lattice defects such as dislocations and disclinations, may lead to a continuous two-stage transition. The distinctive feature of the intermediate phase spanning between the solid and the fluid (the so-called hexatic phase) is the absence of translational order and the presence of quasi-long-range orientational order which eventually spreads out to infinity in the solid phase.

However, apart from liquid crystals and some gases adsorbed on surfaces, the computer simulation of monatomic systems in 2D has not given conclusive evidence of a KTHNY-type behavior: in fact, it seems that in most cases a weak discontinuous transition takes place [11]. In particular, simulated hard disks show a two-phase coexistence region with an estimated jump in density of about 0.04 [12]. One may wonder if and to which extent the indications emerging from numerical experiments are influenced by the standard use of periodic boundary conditions (PBC) on a finite cell, given that such a setup, apart from stabilizing the solid, actually inhibits any loss of coherence at large distances as would be implied by eq. (1.1).

In order to test the importance of these effects, we present in this paper a computer simulation study of a system of hard particles on a sphere, a model which does not interfere with the natural tendency of the infinite system to isotropy. The spherical surface seems a good choice in that it has no boundaries and, therefore, one does not need to invoke PBC. Furthermore, in the limit of infinite radius we recover the infinite plane. The major shortcoming of

such a choice is that extended hexagonal order is ruled out because of the finite curvature. On the other hand, this system may exhibit whatever order it prefers on a local scale. The comparison between samples of a different size may hopefully clarify the behavior of the model when the number of particles grows to infinity at fixed density, thus yielding independent hints on the properties of the infinite flat system at the transition point.

The first computer simulation of hard-disk packings with spherical boundary conditions (SBC) was performed by Schreiner and Kratky [13]. However, this calculation was based on a *non-equilibrium* "successive compression" technique with the stated purpose of producing metastable random-close-packing (RCP) arrangements of a number of particles ranging from 60 to 1600. Such glassy configurations cannot be easily generated within the ordinary flat geometry since the system undergoes a phase transition to the ordered hexagonal phase at a density well below the estimated RCP threshold. More recently, Tobochnik and Chapin carried out a standard Monte Carlo simulation of hard particles on both an ordinary sphere and on the surface of a four-dimensional hypersphere in order to obtain metastable amorphous states at higher densities than previously achieved [14]. The technique adopted by these authors was to increase the diameter of the particles, while keeping the radius of the sphere fixed, so as to produce a state with given density. Typical runs were reported to consist of about 20000 attempted moves per particle. However, on comparing their results on the RCP estimate for the 2D system with those reported in ref. [13], the above authors apparently refer to one single sampled size of 100 particles. At any rate, neither the size dependence of the equilibrium calculation is exploited nor any indication is found of the ordering transition which *must* eventually show up on approaching the flat geometry.

The goal of the present study is to clarify the equilibrium thermodynamic behavior of this model, exploring at the same time the nature of the local order attained by calottes on a sphere at high densities and the way it propagates to greater and greater distances upon increasing the size of the system.

2. Theory

2.1. The model

The system consists of N equal calottes with curved diameter σ and area $2\pi R^2[1-\cos(\sigma/R)]$, R being the radius of the hosting spherical surface. The model Hamiltonian can be written as

$$\mathcal{H} = \sum_{i=1}^{N} \left(\frac{p_{\theta_i}^2}{2mR^2} + \frac{p_{\phi_i}^2}{2mR^2 \sin^2(\theta_i)} \right) + \frac{1}{2} \sum_{i \neq j=1}^{N} v(\alpha_i, \alpha_j) , \tag{2.1}$$

where $\alpha \equiv (\theta, \phi)$ stands for the set of spherical coordinates, p_{θ_i} and p_{ϕ_i} are the canonical momenta of the ith particle, and $v(\alpha_i, \alpha_j)$ is the pairwise interaction potential:

$$v(\alpha, \alpha') = \begin{cases} +\infty & \text{for } r(\alpha, \alpha') < \sigma , \\ 0 & \text{for } r(\alpha, \alpha') > \sigma . \end{cases} \tag{2.2}$$

The spherical distance $r(\alpha, \alpha')$ between two calottes with angular coordinates α and α' is measured along the great circle passing through the particle centers.

2.2. Radial distribution function and equation of state

The radial distribution function (RDF) $g(r)$ is evaluated as:

$$\rho g(r) = \frac{\mathcal{N}(r)}{\mathcal{S}(r)} , \tag{2.3}$$

where $\rho = N/4\pi R^2$ is the number density, $\mathcal{N}(r)$ is the average number of particles lying within a spherical ring (centered on a reference particle) with curved radius r, thickness $\Delta r \ll r$, and area $\mathcal{S}(r) = 2\pi R \sin(r/R)\, \Delta r$.

The pressure P is obtained as:

$$\frac{\beta P}{\rho} = 1 + \frac{1}{2} \pi \sigma^2 \left[\frac{R}{\sigma} \sin\left(\frac{\sigma}{R} \right) \right] g(\sigma) , \tag{2.4}$$

where $g(\sigma) \equiv \lim_{r \to \sigma^+} g(r)$, and β is the inverse temperature in units of Boltzmann's constant. Note that, as $\sigma/R \to 0$, eq. (2.4) yields the equation of state (EOS) of a system of hard disks.

2.3. Voronoi tessellation

In order to describe the local structure in terms of bond-angle correlations and point defects we need to identify the nearest neighbors of each particle. The Voronoi construction is the most natural way to define a set of neighbors for the points of a disordered array. The Voronoi cell associated with the particle at site P is defined as the set of points of the spherical surface which are closer to P than to any other particle. On a plane, the cell would be a polygon; on the sphere it is still a polygon which however follows the curvature of the surface, the number of sides yielding the particle coordination number. In order to set the boundaries of such a region for a given configuration of the

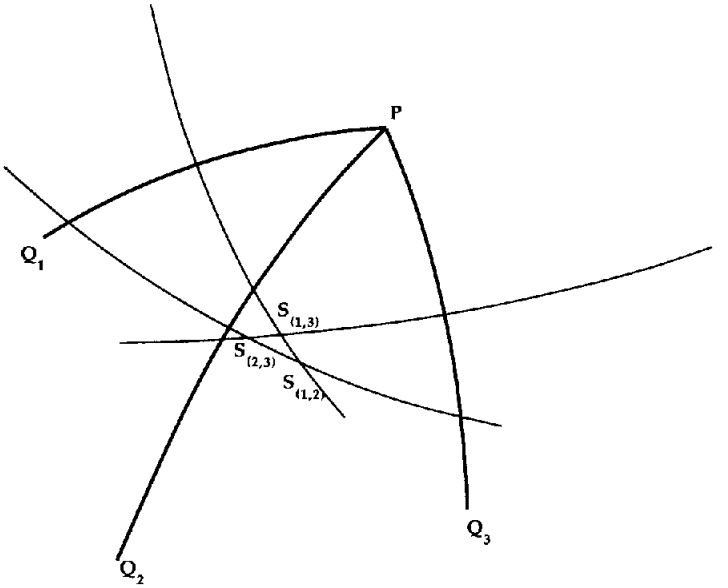

Fig. 1. Geometrical construction carried out on the sphere in order to identify the vertices of the Voronoi polygon associated with particle P (see text).

system, we begin by selecting the twelve sites Q_i which are closest to P. We then calculate the middle point M of each "segment" QP and the points S (their number is $12(12-1)/2 = 66$) at which the "axes" of each distinct pair of segments cross each other (see fig. 1). Let the point $S_{(i,j)}$ correspond to the pair (Q_i, Q_j). Obviously, the axes which we are referring to are great circles intersecting at two diametrically opposite points: S is chosen as the intersection point which is found closest to P. If a point $S_{(i,j)}$ happens to be closer to a point Q (different from Q_i and Q_j) than to P (as points $S_{(1,2)}$ and $S_{(2,3)}$ in fig. 1), it will be removed from the set $\{S\}$. Therefore, this set (which initially contains 66 elements) progressively contracts: the points which are left over at the end of this procedure are nothing but the vertices of the Voronoi polygon whose number is also the coordination number of the reference particle at P. If this number is different from 6, we say that the particle is a disclination. A pair of "bound" (i.e., adjacent) fivefold and sevenfold coordinated disclinations represents a dislocation.

2.4. *Orientational correlation functions*

We define the orientational correlation functions (OCF) as

$$h_n(r) = \langle \cos\{n[\theta(\boldsymbol{r}') - \theta(\boldsymbol{r}'')]\} \rangle \,. \tag{2.5}$$

In eq. (2.5), $r = R \arccos(\boldsymbol{r}' \cdot \boldsymbol{r}'')$ is the spherical distance between the particles whose position on the sphere is defined by the unit vectors $\boldsymbol{r}'$ and $\boldsymbol{r}''$; $\theta(\boldsymbol{r}')$ is the angle, measured on the plane tangent to the sphere at $\boldsymbol{r}'$, between the projections of the line joining the particle at $\boldsymbol{r}'$ with a nearest neighbor (chosen at random among those identified through the Voronoi construction), and of the oriented arc connecting $\boldsymbol{r}'$ to $\boldsymbol{r}''$ along the geodesic. We evaluate the function $h_n(r)$ for $n = 5$, 6, 7. In a flat hexagonal lattice, the difference $\theta(\boldsymbol{r}') - \theta(\boldsymbol{r}'')$ is always a multiple of $\pi/3$ so that, while the functions $h_5(r)$ and $h_7(r)$ vanish everywhere, $h_6(r)$ is one at the lattice distances and zero otherwise. The deviations of these functions from such values show how hexagonal-type angular correlations build up on the sphere with increasing densities and how they decay with distance as a result of the disorder induced in the system by both the equilibrium atomic dynamics and the finite curvature of the embedding space.

3. Simulation

We carried out a Monte Carlo canonical sampling keeping β, N, and ρ constant. At the lowest density, the initial configuration was obtained by placing the particles along equidistant parallels. Then, in order to increase the value of ρ, the sphere radius R was reduced adiabatically starting from the last configuration produced in the run at the immediately lower density. The Monte Carlo configurations were generated by moving one particle at a time at random and rejecting states with overlapping calottes. The maximum amplitude allowed for a move was chosen so as to make the equilibrium acceptance ratio about 0.5. The total number of moves per particle increased from 24000 to 64000 with increasing densities. The canonical averages were computed over 1000 configurations, each of them being extracted every $2N$ moves out of the final segment of the run. Space-dependent functions were calculated with a spatial resolution $\Delta r = 0.05\sigma$.

4. Results

4.1. Thermodynamic properties

The Monte Carlo analysis was performed for three values of the number of particles N, namely 400, 1000, and 2000. In order to evaluate the pressure through eq. (2.4), we need to compute the contact value of the RDF. To this end, we resorted to an exponential fit of $g(r)$ in the close neighborhood of

$r = \sigma$, where the RDF was calculated by performing a more refined average over a segment of 8000 configurations per particle. The resulting values of the compressibility factor $Z(\rho) \equiv \beta P/\rho$ are given in table I. In fig. 2 we show the comparison between $\beta P(\rho)$ for $N = 2000$, a fit of the SBC data computed by Tobochnik and Chapin which is based on eq. (3.2) of ref. [14] and the EOS of the hard-disk (HD) fluid referring to a system of 5822 particles [15]. We first note that the calculated EOS of calottes on a sphere faithfully reproduces the flat-system branch all over the range covered by the data reported by Erpenbeck and Luban ($0 \leq \rho\sigma^2 \leq 0.83$). It is apparent that for such densities the thermodynamic behavior of the particles with SBC does not differ appreciably from that observed on a plane. Hence, it is natural to infer that the local order

Table I
Compressibility factor $\beta P/\rho$ as a function of density for $N = 400$, 1000 and 2000.

$\rho\sigma^2$	N		
	400	1000	2000
0.300	1.731		
0.400	2.146		
0.500	2.792		
0.600	3.693		
0.650	4.284		
0.700	5.141		
0.750	6.098		6.096
0.800	7.473		
0.810			7.767
0.820			8.121
0.830	8.460	8.469	8.488
0.840		8.853	8.832
0.850	9.253	9.275	9.242
0.860		9.646	9.643
0.865		9.823	9.831
0.870		10.291	9.932
0.875			10.166
0.880	10.820	10.606	10.279
0.885			10.513
0.890	11.004	10.758	10.666
0.895			10.785
0.900	11.439	11.263	11.065
0.905			11.073
0.910	12.191	11.563	11.232
0.915			11.525
0.920	12.565	12.240	11.687
0.925			11.966
0.930	11.321	12.719	
0.940	13.996	13.437	
0.950	14.941	14.204	

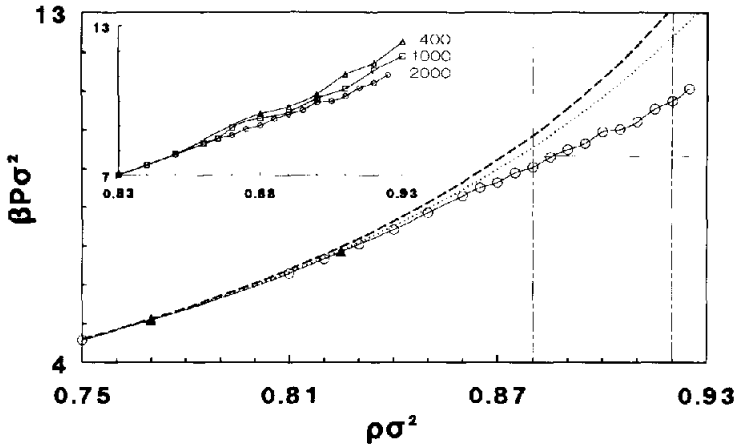

Fig. 2. Equation of state of hard calottes on a sphere. The open circles represent the reduced pressure for the system with 2000 particles. The continuous line is a spline interpolation of the present data. For comparison, we also report the data obtained by Tobochnik and Chapin as fitted through eq. (3.2) of ref. [14] (dashed line), and the data for 5822 hard disks on a plane (solid triangles) with the corresponding Levin approximant based on the first six terms of the virial series (dotted curve) [15]. The tie line at $\beta P\sigma^2 = 8.08 \times 2/\sqrt{3}$ joining the freezing and melting points along the hard disk EOS is also shown [12]. The inset shows the dependence on the size of the system: triangles, 400 particles; squares, 1000 particles; circles, 2000 particles.

built up so far on the sphere does not extend to distances large enough for the spherical curvature to become influential. For $\rho\sigma^2 > 0.83$ and up to the HD freezing density $\rho_F\sigma^2 = 0.88$ [12], the present values for the pressure turn out to be slightly lower than those pertaining to the HD model. This conclusion follows from the comparison between the hitherto accepted value of the transition pressure for disks (9.33 in units of σ^2) and the value (9.05 for $N = 2000$) we find for $\rho = \rho_F$. By contrast, beyond the HD melting point $\rho_M\sigma^2 = 0.92$ [12], the calotte EOS lies above the HD crystal branch. Before attempting an interpretation of these findings, we add a comment on the data of ref. [14]: the values reported there for the pressure turn out to be systematically greater than both the present values and those pertaining to the HD model. This discrepancy is presumably due to a size effect as can be argued from Fig. 2 (inset) showing the EOS for the three samples we have investigated. A neat dependence on the size of the system starts to be observed for $\rho\sigma^2 \gtrsim 0.86$: the pressure decreases with increasing N and undergoes a series of undulations which appear to damp gradually for $\rho\sigma^2 \gtrsim 0.91$. Such a wavy behavior does not show up in the data reported in ref. [14]. However, from fig. 1 of that paper, it appears that the points are located on a rather loose density mesh with an interval of about 0.06 in the region of interest. By contrast, our runs were carried out with a step in density of 0.01 for $N = 400$, 1000 and 0.005

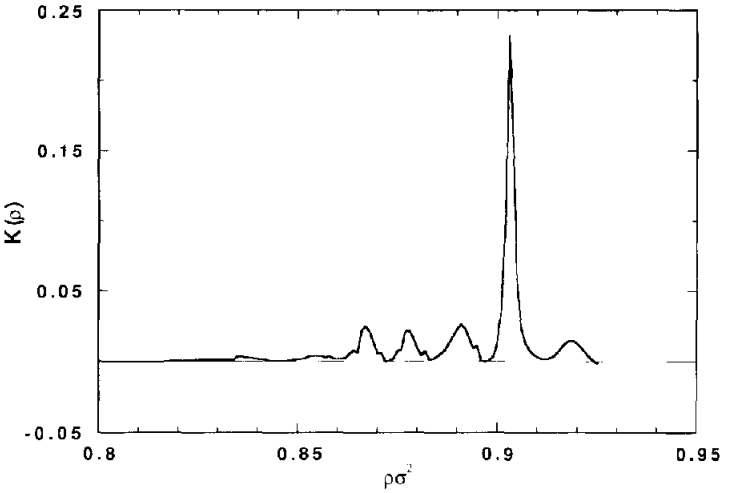

Fig. 3. Reduced isothermal compressibility $K(\rho) \equiv (\partial \beta P / \partial \rho)_\beta^{-1}$ for $N = 2000$, plotted as a function of $\rho\sigma^2$ after the subtraction of an unstructured "background" value extracted from the Levin approximant which is shown in fig. 2.

for $N = 2000$. Correspondingly, a series of peaks appears in the reduced isothermal compressibility of the model $K(\rho) \equiv (\partial \beta P / \partial \rho)_\beta^{-1}$, which is plotted in fig. 3 for $N = 2000$ after subtracting a monotonously decreasing "background" value which is extrapolated from low densities through the Levin approximant shown in fig. 2 [15]. The most outstanding feature is the pronounced maximum located at $\rho\sigma^2 = 0.905$, which is also preceeded by a number of minor satellite peaks.

On the basis of the above evidence on the thermodynamic properties of the model, we can tentatively identify three different packing regimes

(1) a low-density fluid regime for $\rho\sigma^2 < 0.86$ characterized by the absence of sensitive curvature effects and ordering phenomena;

(2) an intermediate-density regime for $0.86 < \rho\sigma^2 < 0.91$ where the system manifests some sort of "criticality" which unveils through the dependence of the data upon the size of the system;

(3) a high-density regime for $\rho\sigma^2 > 0.91$ which follows what appears to be a continuous transition towards a spatially organized phase.

4.2. *Radial distribution function*

In fig. 4 we present the RDF of 2000 calottes at short distances for a number of densities in the range of interest. The curves are plotted as a function of r/a, where $a = \sigma(\rho_{CP}/\rho)^{1/2}$ is the hexagonal lattice constant on a plane and $\rho_{CP}\sigma^2 = 2/\sqrt{3}$ is the corresponding close-packing density. The structural coun-

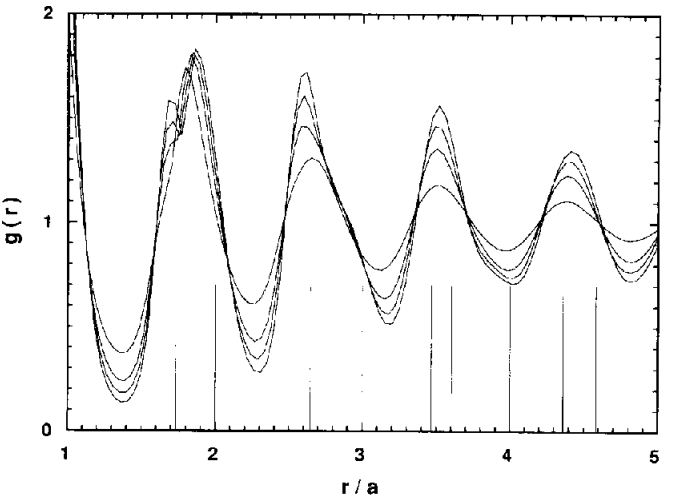

Fig. 4. Radial distribution function of 2000 calottes plotted for increasing densities ($\rho\sigma^2 = 0.86$, 0.895, 0.91 and 0.925) as a function of r/a, where a is the hexagonal lattice constant on a plane. The vertical lines identify the characteristic distances in the ideal hexagonal lattice ($r/a = 1, \sqrt{3}, 2, \sqrt{7}, 3, 2\sqrt{3}, \sqrt{13}, 4, \sqrt{19}, \sqrt{21}, 5, \ldots$).

terpart of the major inflection observed in the EOS for $\rho\sigma^2 \simeq 0.91$ is the outbreak, on a local scale, of ordered patches with hexagonal symmetry. In fact, it is at such a density that all the characteristic distances of the triangular lattice up to the sixth shell of neighbors become manifest in the RDF profile.

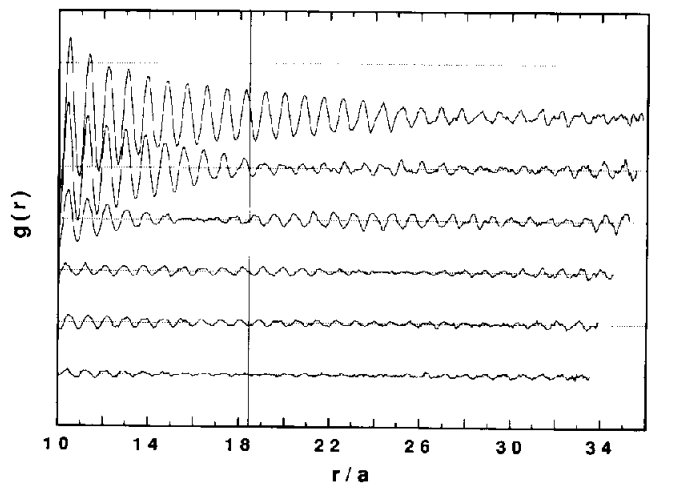

Fig. 5. Asymptotic behavior of the radial distribution function of 2000 calottes plotted as a function of r/a for densities $\rho\sigma^2 = 0.81$, 0.83, 0.86, 0.895, 0.91 and 0.925. Density increases from bottom to top, and each successive curve is displaced upwards by 0.05 for clarity. The vertical line drawn for $r/a = \frac{1}{4}(\pi N/\rho_{CP}\sigma^2)^{1/2}$ marks the position of the equator with respect to the pole at $r = 0$.

In particular, we note the splitting of the maximum centered about $r/a \simeq 1.8$ into a pair of adjacent peaks corresponding to the second and third coordination shell, respectively, and the resolution of the lattice fifth shell which is unraveled by the appearance of a shoulder for $r/a \simeq 3$. The existence of distinct packing regimes can also be argued from an inspection of the asymptotic behavior of the RDF. As is seen from fig. 5, upon increasing the density, the expected long-range decay of $g(r)$ acquires an extra modulation with period much greater than σ. This feature appears to set in for $\rho\sigma^2 \simeq 0.83$ and is particularly apparent for $\rho\sigma^2 = 0.895$ where a large-wavelength oscillation clearly persists beyond $r/a \simeq 16$ through the initial exponential decay of the RDF maxima. For densities greater than 0.91, which again plays the role of a borderline case, the shape of the RDF shows the extensive propagation of spatial correlations up to πR, which is the maximum distance allowed on the sphere. In fact, for $\rho\sigma^2 = 0.925$ it turns out that the asymptotic decay of this

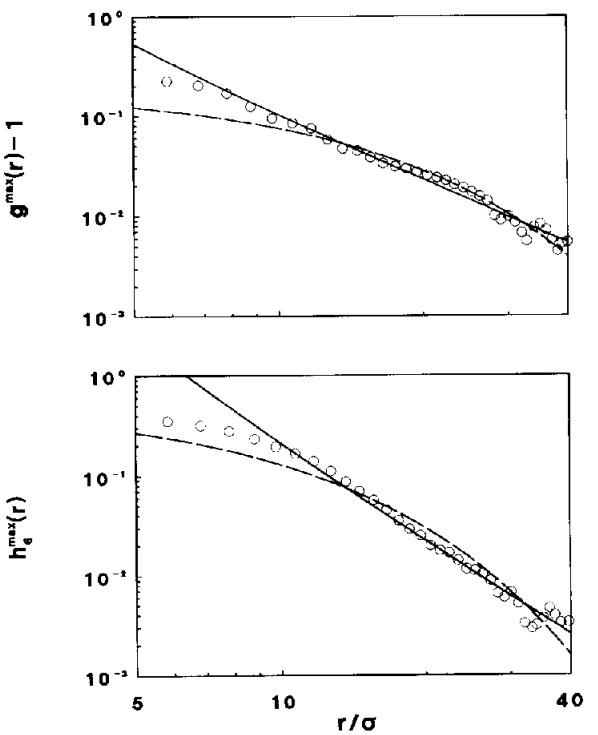

Fig. 6. Maxima of the radial distribution function and of the orientational correlation function plotted as a function of r/σ on a log–log scale for $\rho\sigma^2 = 0.925$ and $N = 2000$. The solid lines represent best fits to algebraic decay in the range $9\sigma \leqslant r \leqslant 40\sigma$ with exponents 2.02 and 3.02 for $g(r)$ and $h_\theta(r)$, respectively. The dashed lines are the results of a best fit to an exponential decay over the same range of distances with spatial decay lengths of 10.14σ and 6.80σ, respectively.

function is no longer exponential but more distinctly algebraic: as can be appreciated from fig. 6, the locus of maxima in the range $9\sigma \lesssim r \lesssim 40\sigma$ can be fitted to a form $A/(r-\sigma)^n$ with an inverse power-law exponent $n \simeq 2$. Furthermore, the superimposed modulation in the RDF profile appears to be more complex than at lower densities. We conclude that for $\rho\sigma^2 = 0.91$ the system undergoes a transition from a fluid to a solid-like phase with quasi-long-range translational order.

4.3. *Orientational correlation functions*

The orientational correlation functions are more sensitive probes of the local structure than the radial distribution function since their operational definition involves the relative arrangement of four particles. In particular, the function $h_6(r)$ is a fine indicator of the emergence of hexagonal patterns in the system as is seen from fig. 7 where this quantity is drawn for increasing densities, together with the positions which particles would attain on a triangular lattice. The spatial resolution of the second and third shell of neighbors is already present for $\rho\sigma^2 = 0.75$, well below the claimed transition point. At variance with the RDF, even the mean nearest-neighbor separation distinctly shows up in $h_6(r)$. We also note that, across the ordering transition, the eighth coordination shell of the hexagonal lattice emerges out of a dip region.

The presence of such a detailed fine structure in the sixfold OCF in the fluid region demonstrates that the angular correlations pertaining to a hexagonal texture appear well before their positional counterpart. For $\rho\sigma^2 \gtrsim 0.86$ this

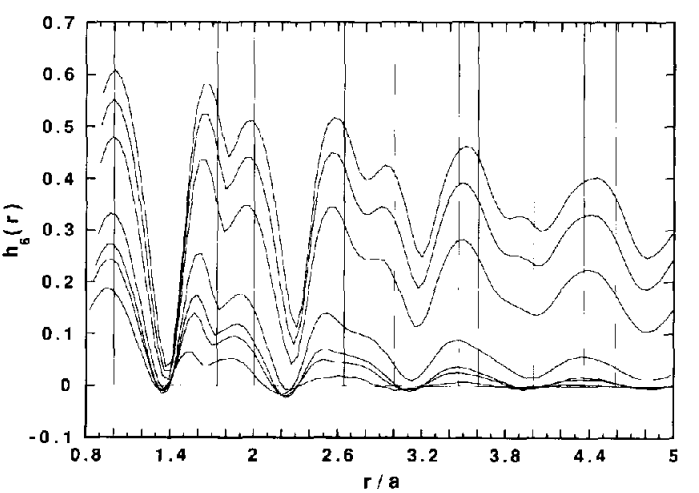

Fig. 7. Orientational correlation function $h_6(r)$ of 2000 calottes plotted for increasing densities ($\rho\sigma^2 = 0.75$, 0.81, 0.83, 0.86, 0.895, 0.91 and 0.925) as a function of r/a. The vertical lines identify the characteristic distances in the ideal hexagonal lattice (see fig. 4).

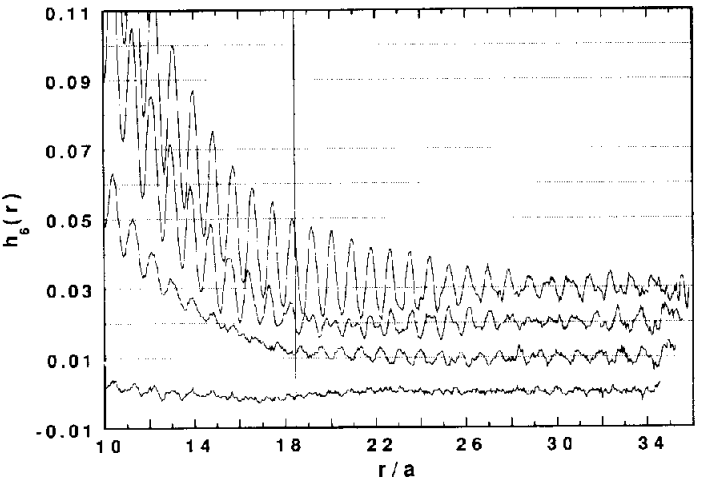

Fig. 8. Asymptotic behavior of the function $h_6(r)$ of 2000 calottes plotted as a function of r/a for densities $\rho\sigma^2 = 0.86$, 0.895, 0.91 and 0.925. Density increases from bottom to top, and each successive curve is displaced upwards by 0.01 for clarity. The vertical line marks the position of the equator.

function stops oscillating about zero and remains positive definite for a very wide range of distances (see fig. 8). The rationale behind this is that, inside such an interval, the angle between two bonds may not differ, on the average, from a multiple of $\pi/3$ for more than $\pi/12$. This means that the system soon acquires a sort of orientational *rigidity* which is not based on a definite fixing of the distances of successive neighbor shells from a generic reference particle. The size of the angularly coherent domains increases with the number of particles N. At the highest densities, it settles down at about 20σ for $N = 2000$.

This type of order recalls that of a hexatic fluid. However, there apparently is no well-defined transition in this model system from the disordered fluid into a hexatic phase although, as noted above, for $\rho\sigma^2 \gtrsim 0.86$ orientational correlations blow up both in amplitude and in spatial extension. Also the analysis of the asymptotic behavior of $h_6(r)$ does not provide a conclusive answer: as for the RDF, for $\rho\sigma^2 \lesssim 0.91$ the decay seems to be consistent with an exponential form, while for $\rho\sigma^2 = 0.925$ an inverse-power law with an exponent $n \simeq 3$ reproduces the upper envelope of the function better over a wider range of distances (see fig. 6).

We finally present $h_5(r)$ and $h_7(r)$ in fig. 9. Both these functions oscillate systematically about zero and yield comparatively much smaller values than $h_6(r)$. The most relevant structures are the negative dips which fall exactly in the interstitial regions between successive coordination shells with prevalent hexagonal geometry. In such regions, the peculiar average value of $\cos(5\Delta\theta)$

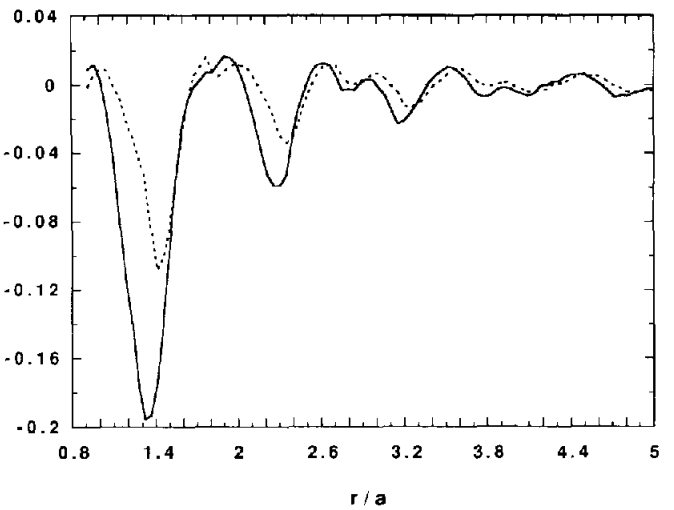

Fig. 9. Orientational correlation functions $h_5(r)$ (dotted line) and $h_7(r)$ (continuous line) of 2000 calottes plotted as a function of r/a at reduced density 0.925.

and $\cos(7\Delta\theta)$ is the outcome of a delicate balance between positive and negative contributions arising from pairs of nearest-neighbor bonds in defective clusters.

5. Discussion

The evidence attained through the thermodynamic and structural data presented in this model study of hard calottes on a sphere indicates that, in spite of the frustration effect induced by the topology of the host surface, this system most clearly undergoes a phase transition at a reduced density close to 0.91. Below the transition point, the state of the system shows a high level of orientational coherence which settles in at $\rho\sigma^2 \simeq 0.86$, when the properties of the model already show a neat dependence on the total number of particles. We surmise that the achievement of this intermediate level of ordering is responsible for the lower pressure which is observed on the sphere as compared to the hard-disk value at a given density. However, notwithstanding the fairly extended range of the hexagonal correlations, the nature of the asymptotic behavior of the angular distribution function does not comply with the ordinary definition of a hexatic phase on a plane. Actually, the decay of both the orientational and radial distribution functions becomes algebraic beyond the transition point, suggesting the emergence of extended solid-like order in the system. As already noted in the preceding section, the shape of these

functions indicates the formation of large hexagonal domains which are easily seen in the equilibrium snapshot presented in fig. 10, taken for $\rho\sigma^2 = 0.925$.

It is possible to predict the maximum size which such a domain may attain at a given density on the basis of a heuristic argument which follows straight from the existence of an instability threshold for the isotropic propagation of hexagonal order on a sphere of radius R. Suppose we want to dispose as many rings of hexagonally coordinated particles as possible around a reference calotte located at, say, the north pole of the sphere. Let a_n (with $n = 1, 2, \ldots$) be the distance of the vertices of the nth curved hexagon from the fixed particle. These points lie along meridian lines forming angles of $\pi/3$. Let particles be distributed with pace d_n along the geodetic arcs $\mathscr{L}_n$ which join pairs of adjacent vertices. The length l_n of such segments is:

$$l_n = R \arccos[1 - \tfrac{1}{2} \sin^2(a_n/R)] . \tag{5.1}$$

On a plane, n particles can be accommodated within $\mathscr{L}_n$ with constant spacing $d_n = a$ if, as in the case of the ideal triangular lattice, $a_n = na$. On a sphere, the

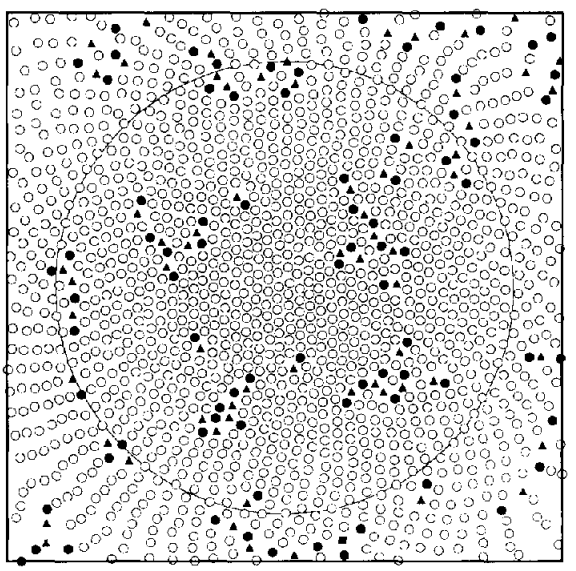

Fig. 10. Projection onto a plane of the particle positions extracted from a typical configuration of 2000 calottes with a reduced density $\rho\sigma^2 = 0.925$. The polar coordinates (r', ϕ') of the point corresponding through the projection to the position of a calotte with spherical coordinates (R, θ, ϕ) are obtained as $r' = R\theta$, $\phi' = \phi$. Different symbols are used to distinguish particles with five neighbors (solid circle), six neighbors (open circle), seven neighbors (solid triangle), and eight neighbors (solid square) in the Voronoi construction. The continuous line marks the position of the equator. We note that, upon moving away from the pole, interparticle distances get more and more distorted as a result of the planar projection.

two constraints $a_n = na$ and $l_n = na$ cannot be fulfilled simultaneously. In particular, if we choose $a_n = na$, it turns out that $l_n < na$. Moreover, this length decreases monotonously with n so that it is possible to determine a value n_1 such that l_n is eventually less than $(n-1)a$. Therefore, upon moving away from the pole, the particles placed on the nth ring will get closer and closer until one particle must be expelled out of the ring if we want to restore the proper original pace a. This mechanism, which is strictly associated with finite curvature effects, will force the formation of disclinations in excess of those which are ordinarily produced by equilibrium thermal excitations. When the above condition occurs, the hexagonal tessellation is definitely ruled out. The value $n_1 a$ can then be taken as an upper bound of the radius R_D of the biggest ordered domain which can grow on the sphere. Should l_n become less than $n\sigma$ for a value of n smaller than n_1, the estimated upper-bound value of R_D would be even lower. However, this will happen only for values of $N \lesssim 1400$. We also note that n_1 depends only upon the ratio R/a, a number which, for given N, does not vary with the density.

On the other hand, we can fix the value of $l_n = na$ and determine a_n. In this case $a_n > na$; furthermore, since the distance between two successive rings grows with n, peripheral hexagonal cells become more and more stretched along the radial direction. When a_n becomes bigger than $(n+1)a$ as a result of the above constraint on d_n, the structure becomes unstable since, via a suitable collective rearrangement along the radial direction, another ring of particles might potentially be accommodated. This condition defines another upper threshold for n, say, n_2. It turns out that the N-dependent ratio n_1/n_2 rapidly tends to 1 for increasing values of N. for $N = 2000$, just beyond the transition point, we find $n_1 = 11$ and $n_2 = 10$. Indeed, a look at the central domain in fig. 10 confirms the validity of the above prediction. This circumstance is also fully consistent with the reported behavior of the sixfold OCF which shows a characteristic length of about 20σ, the "diameter" of a typical ordered path. The predictions offered by both instability criteria are also fully consistent with the data obtained for lower values of N.

The radius of the ordered domains, as can be estimated through the above criteria, depends on the total number of particles as:

$$R_D \sim N^{1/3}. \tag{5.2}$$

However, the algebraic decay of the correlation functions for $\rho \gtrsim 0.91$ clearly indicates the extensive propagation of both translational and orientational order through the whole surface. Therefore, defects forming along the borderline regions between adjacent domains do not enfold them entirely. Localized

clusters of defects arise, allowing hexagonal order to percolate through contiguous domains until a connected structure is established all over the sphere. The necessity of such a large-scale frame does actually respond to a criterion of efficiency in the way six-fold coordinated particles pack on a sphere. In fact, the equilibrium state of infinitely repulsive particles is the state of maximum entropy for a given volume and number of particles, a condition which, at high densities, is fulfilled by resorting to a hexagonal tessellation of the space. On a sphere this solution cannot be pursued indefinitely because of the upper bound on the size of ordered domains. We surmise that, as a result of this constraint, the most efficient and regular coverage of the entire surface will likely be attained when such ordered patches become centered at the vertices of the Platonic polyhedron inscribed within the sphere which better fits the value of R_D. Disclinations induced by the finite curvature will then mostly segregate in the space left over between domains. For $N = 2000$ and $\rho = 0.925$, this criterion would suggest the octahedron as the supporting frame of the whole structure. In fact, among the five regular polyhedra, it is in the octahedron that the curved radius of the circular regions drawn on the sphere ($\pi R/4 \simeq 10.3\sigma$) gives a value which is closest to the estimate previously obtained for R_D. Indeed, if one looks at fig. 10, it is possible to envisage a large fragment of such a "superstructure" in the four clusters of defects which delimit the central domain from the neighboring ones.

This scenario will change with the number of particles present in the system: in fact, for increasing values of N, the angle subtended by each domain decreases as $N^{-1/6}$. We presume that, on account of the isotropy properties of the system, the superstructures sequentially generated on the sphere with growing N will be endowed with a symmetry group whose order is the highest compatible with the number of vertices. We then expect that the system will realize new optimal surface coverings by first calling into play Platonic polyhedra other than the octahedron. Among these, we note that the densest regular mapping on the sphere is provided by the icosahedron. Its symmetry group will likely furnish the asymptotic underlying framework for further more complex dense coverings involving a higher and higher number of domains as suggested by the study of isogonal tilings on the sphere [16,17].

In closing, we should like to note that a conceptually similar situation has recently been discussed for a two-dimensional Ising spin system embedded on the surface of a Möbius strip [8]. This topology is most clearly a source of frustration for the global orientation of the spins. In spite of such an anomalous geometrical setup, the authors report the onset of spontaneous magnetization which results in the formation of macro-domains with a coherent spin direction. Furthermore, consistently with the present findings, the transition appears to be less sharp than in standard Monte Carlo simulations with PBC.

6. Concluding remarks

The nature of the mechanism responsible for the onset of the peculiar high-density phase described above furnishes probatory evidence for the continuous character of the fluid–solid transition on a sphere. The transition signals the outgrowth in the system of an upper level of organization following the clearcut definition of hexagonally ordered domains. As such, this process would not imply a discontinuous contraction across the transition of the phase-space region available to the system. Obviously, the above phenomenology may not be trivially transposed to a flat geometry even in the thermodynamic limit. However, in the light of the Peierls–Landau argument on the absence of true crystalline long-range order in two dimensions, one might envisage an analogy between the two geometries in the compelling existence of correlation regions whose size grows more slowly than the size of the system. If so, the present results would cast a shadow on the claimed discontinuous nature of the transition undergone by hard particles on an infinite plane.

We reserve to a forthcoming paper a more detailed analysis of the thermodynamics and structure of point defects in this model.

Acknowledgements

This work was supported by the Ministero dell'Università e della Ricerca Scientifica e Tecnologica, and by the Consorzio Interuniversitario Nazionale per la Fisica della Materia. The authors would also like to thank the Consiglio Nazionale delle Ricerche for the allocation of computer time via the Cray project on statistical mechanics.

References

[1] R. Peierls, Helv. Phys. Acta Suppl. ii (1936) 81.
[2] L.D. Landau and E.M. Lifshitz, Statistical Physics (Addison–Wesley, Reading MA, 1969).
[3] N.D. Mermin, Phys. Rev. 176 (1968) 250.
[4] W.G. Hoover, W.T. Ashurst and R.J. Olness, J. Chem. Phys. 60 (1974) 4043.
[5] F. Bavaud, Ph. Choquard and J.-R. Fontaine, J. Stat. Phys. 42 (1986) 621.
[6] K. Binder, in: Monte Carlo Methods in Statistical Mechanics, K. Binder, ed. (Springer, Berlin, 1979), p. 22.
[7] N. Jan and M.O. Steinitz, J. Stat. Phys. 30 (1983) 37.
[8] H. Ito and T. Sakaguchi, Phys. Lett. A 160 (1991) 424.
[9] J.M. Kosterlitz and D.J. Thouless, J. Phys. C 6 (1973) 1181.
[10] D.R. Nelson and B.I. Halperin, Phys. Rev. B 19 (1979) 2457.
A.P. Young, Phys. Rev. B 19 (1979) 1855.

[11] K.J. Strandburg, Rev. Mod. Phys. 60 (1988) 161.
[12] W.G. Hoover and F.H. Ree, J. Chem. Phys. 49 (1968) 3609.
[13] W. Schreiner and K. Kratky, J. Chem. Soc., Faraday Trans. 2, 78 (1982) 379.
[14] J. Tobochnik and P.M. Chapin, J. Chem. Phys. 88 (1988) 5824.
[15] J.J. Erpenbeck and M. Luban, Phys. Rev. A 32 (1985) 2920.
[16] B. Grünbaum and G.C. Shephard, in: The Geometric Vein: The Coxeter Festschrift, C Davis, B. Grünbaum and F.A. Sherk, eds. (Springer, Berlin, 1981), p. 65.
[17] T. Tarnai, J. Mol. Biol. 28 (1991) 485.